Collapse and control of the MnAu$_2$ spin-spiral state through pressure and doping

J. K. Glasbrenner

National Research Council/Code 6393, Naval Research Laboratory, Washington, DC 20375, USA

MnAu$_2$ is a spin-spiral material with in-plane ferromagnetic Mn layers that form a screw-type pattern around a tetragonal c axis. The spiral angle θ was shown using neutron diffraction experiments to decrease with pressure, and in later studies it was found to suffer a collapse to a ferromagnetic state above a critical pressure, although the two separate experiments did not agree on whether this phase transition is first or second order. To resolve this contradiction, we use density functional theory calculations to investigate the spiral state as a function of pressure, charge doping, and also electronic correlations via a Hubbard-like U. We fit the results to the one-dimensional J_1-J_2-J_3-J_4 Heisenberg model, which predicts either a first- or second-order spiral-to-ferromagnetic phase transition for different regions of parameter space. At ambient pressure, MnAu$_2$ sits close in parameter space to a dividing line separating first- and second-order transitions, and a combination of pressure and electron doping shifts the system from the first-order region into the second-order region. Our findings demonstrate that the contradiction in pressure experiments regarding the kind of phase transition are likely due to variations in sample quality. Our results also suggest that MnAu$_2$ is amenable to engineering via chemical doping and to controlling θ using pressure and gate voltages, which holds potential for integration in spintronic devices.

I. INTRODUCTION

The tetragonal material MnAu$_2$ is one of the oldest known spin-spiral materials [1–3], with a Néel temperature of $T_N = 363$ K [1] and a local Mn moment of $3.5\mu_B$ [3,4]. The magnetic ground state consists of in-plane ferromagnetic Mn layers with a screw-type pattern around the tetragonal c axis, which can be described using a spiral angle θ [this is equivalent to the wave vector $\mathbf{q} = (0,0,q_z)$, where $\theta = q_z c/2$]. Neutron diffraction measurements [3,5,6] find that θ has a weak dependence on temperature, increasing slightly with increasing temperature [$\theta(77$ K$) = 47°$ and $\theta(295$ K$) = 51°$]. The spiral state is known to collapse to a metamagnetic fanlike configuration when placed in a $\sim$10 kOe magnetic field at room temperature [1,2], which led to a revival of interest in MnAu$_2$ when it was found that this gives rise to a giant magnetoresistive effect [4].

There are several microscopic mechanisms that can induce spin spirals. In itinerant systems, both Fermi surface nesting [7] and the Ruderman-Kittel-Kasuya-Yosida (RKKY) interaction [8–10] can lead to spiral formation. The Dzyaloshinsky-Moriya (DM) interaction [11,12], which occurs in materials without an inversion center (MnAu$_2$ has an inversion center, which rules it out as a possible mechanism), can also induce spirals and moment canting, but due to the interaction's relativistic origin it is more important in materials with heavy elements. It can still be competitive in lighter transition metals, such as MnSi [13–15], but the spirals will have a long wavelength due to weak relativistic effects. Finally, frustration, which can be geometric or magnetic, can encourage noncollinearity and lead to the formation of spirals.

The spin spirals in MnAu$_2$ are understood to be a consequence of magnetic frustration, which is commonly modeled using a one-dimensional Heisenberg model with first and second neighbor interplanar couplings (the J_1-J_2 model) [16,17]. In this model, the spiral state is stable when $J_1 \neq 0$, $J_2 > 0$, and $|J_1| < 4|J_2|$ [16]. The validity of applying this model to MnAu$_2$ was confirmed using density functional theory (DFT) calculations [18,19]. The origin of the magnetic frustration was traced to a competition between two exchange mechanisms, nearest-neighbor superexchange and a transferred RKKY-like interaction, and electronic correlations were found to play an essential role in suppressing the RKKY-like interaction, which is necessary to satisfy the $|J_1| < 4|J_2|$ inequality [19].

The spiral angle θ is sensitive to pressure, with neutron diffraction measurements determining that $\theta(P)$ decreases with applied pressure [$\theta(0) = 50.7°$ $(47.0°)$ decreasing to $\theta(8.83$ kbar$) = 41.8°$ $(40.5°)$ at a temperature of 295 K (77 K)] [5]. Measurements of the critical magnetic field H_c for the spiral-to-ferromagnetic transition as a function of pressure, when extrapolated to zero external field, implied that the spiral state should collapse to ferromagnetism at $\sim$12 kbar [20]. The pressure-induced spiral-to-ferromagnetic transition was confirmed by subsequent experiments using inductance measurements [21], electrical resistivity measurements, and measurements of H_c [22], although the two reports disagreed on the order of the phase transition. In Ref. [21], the transition is of the second kind and occurs over a pressure range of 12–20 kbar, while in Ref. [22] it is of the first kind and occurs at 13 kbar. This contradiction was never resolved and remained an open question.

The J_1-J_2 Heisenberg model, which can explain the stability of the spiral state, predicts that the transition must be of the second kind. However, general investigations of the classical one-dimensional Heisenberg model show that including the third nearest-neighbor term J_3 leads to regions of parameter space with first order phase transitions [23,24]. Further neighbors, such as J_4, change the area of parameter space where first-order transitions occur [24]. It follows then that if a system were to sit near the boundary in parameter space separating first- and second-order phase transitions, then variations in material quality could shift the system towards one region or the other.

We argue that this is the case for MnAu$_2$. We support this claim using DFT calculations to simulate the effects of pressure, charge doping, and variation in the strength of electronic correlations via a Hubbard-like U. We calculate

the magnetic energies and fit them with a classical, one-dimensional Heisenberg model with coupling between the first four nearest-neighbor Mn planes. We confirm that ideal, stoichiometric $MnAu_2$ sits close to a boundary separating first- and second-order phase transitions, and that varying the pressure and doping shifts $MnAu_2$ across this critical boundary. This suggests that the two pressure experiments are not in conflict, but instead the $MnAu_2$ samples from each are located in two separate portions of phase space. The spiral angle θ is also found to be responsive to applied pressure and doping, which holds promise for integration of $MnAu_2$ into spintronic devices.

II. COMPUTATIONAL DETAILS

We employed DFT to solve the electronic structure of $MnAu_2$ and calculate the total energy of magnetic configurations. To perform these calculations, we used the all-electron code ELK [25], which is an implementation of the full-potential linear augmented planewave method, and also projector augmented wave potentials implemented in the code VASP [26,27]. We used the local spin-density approximation (LSDA) [28] for our calculations, and for correlation effects we used the DFT $+ U$ method in the fully localized limit [29], in which we introduce a Hubbard-like U on the $3d$ orbitals of the Mn atoms. We used two values of U, $U = 3.12$ eV and 4.7 eV, and J was set to 0.7 eV.

$MnAu_2$ has a tetragonal crystal structure with $I4/mmm$ space group symmetry. The experimental lattice parameters are $a = 3.370$ Å and $c/a = 2.599$, yielding a volume of 49.741 Å³/formula unit, and the Wyckoff positions for Mn and Au are $2a$ and $4e$, respectively, with the internal experimental height for Au $z_{Au} = 0.34$ (fractional coordinates) [30,31]. To simulate pressure, we began with the $MnAu_2$ unit cell from experiment with tetragonal symmetry and varied the lattice parameters a and c to set the volume [32]. We then fixed the volume and performed structural relaxations in VASP to optimize the c/a ratio and the internal parameter z_{Au}. After the relaxation, we performed total energy calculations in VASP with the tetrahedron method and calculated the pressure using the formula $P = -dE/dV$. We then imported the relaxed structures into ELK for calculating the magnetic energies.

We employed two methods to simulate charge doping, (1) adding electrons directly to the system along with a uniform positive charge background (hereafter referred to as "charge dosing"), and (2) using the virtual crystal approximation (VCA). The VCA involves replacing the Au ions with fictitious ions of fractional charge in order to add electrons or holes to the system. We used the experimental lattice parameters of $MnAu_2$ in our doping calculations, while for calculations with simultaneous charge doping and applied pressure we used the relaxed cells obtained with VASP.

We used the spin spiral method implemented in ELK to calculate the total energy as a function of the spiral angle. This method defines a wave vector $\mathbf{q} = (0,0,q_z)$ that is applied to a primitive cell to simulate spirals. In our previous study of $MnAu_2$ [19], we found good agreement between the calculated energies obtained via this method and noncollinear calculations of spirals in supercells. In this study, our procedure was to calculate the energy as a function of the wave vector

for the range $0 < q_z < 2\pi/c$ as we varied the pressure, charge doping, and Hubbard U. We then used $\theta = q_z c/2$ to convert the wave vector to an angle.

Convergence for the spin spiral calculations was carefully checked in the primitive cells, and the following parameters were necessary to achieve convergence: k-mesh $= 16 \times 16 \times 16$, nempty $= 8$, rgkmax $= 8.0$, gmaxvr $= 12$, lmaxapw $= 8$, and the smearing function width was set to 0.0001 Ha.

III. SUMMARY OF 1D HEISENBERG MODEL

The magnetic interactions in $MnAu_2$ are typically modeled using the Heisenberg model:

$$H = \sum_{i \neq j} J_{ij} \hat{\mathbf{m}}_i \cdot \hat{\mathbf{m}}_j. \tag{1}$$

Note that $J_{ij} = \bar{J}_{ij} |\mathbf{m}|^2$, where $\bar{J}_{ij}$ is the magnetic coupling and $|\mathbf{m}|$ is the moment amplitude. DFT calculations confirm that Mn is in the high spin state with $S = 5/2$, which makes the classical Heisenberg model suitable for studying the magnetic interaction. The magnetic moment is also assumed to be constant, which is reasonable as the Mn moment amplitudes do not vary by much as a function of θ.

The spiral state of $MnAu_2$ is completely described by the parameter θ. As a result, we can simplify the Heisenberg model to one dimension:

$$E(\theta) = \frac{H}{N} = \text{const.} + \sum_{n=1}^{m} J_n \cos(n\theta), \tag{2}$$

where N is the total number of Mn planes and m is the maximum number of nearest-neighbor couplings to be included in the model. The interplanar coupling determines the spiral state stability, and below we discuss the phase diagram for the models which include two (J_1-J_2 model, $m = 2$), three (J_1-J_2-J_3 model, $m = 3$), and four (J_1-J_2-J_3-J_4 model, $m = 4$) nearest-neighbors in Eq. (2).

The J_1-J_2 model is the simplest possible model with a stable spiral state, which occurs when $J_1 \neq 0$, $J_2 > 0$, and $|J_1| < 4|J_2|$. The angle θ is plotted as a function of $J_2/|J_1|$ in Fig. 1(a), and the spiral-to-ferromagnetic phase transition is of second order. What has not been appreciated in previous studies of $MnAu_2$ is that this model cannot explain how the turn angle could collapse under pressure in a first-order transition, as measured in Ref. [22].

Including the third nearest-neighbor coupling yields the J_1-J_2-J_3 model, which can be solved analytically (see Supplemental Material [33]) [23,24]. The phase diagram of θ for this model as a function of $J_2/|J_1|$ and $J_3/|J_1|$ is depicted in Fig. 1(b). There are two regions in the parameter space, the ferromagnetic region in the lower left and the spiral region in the rest of the diagram, with the contour plot corresponding to the magnitude of θ. The phase boundaries separating the two regions are [23]:

$$J_3 = \begin{cases} \frac{1}{9}(|J_1| - 4J_2) & 0 \leqslant J_2/|J_1| \leqslant 2/5 \\ \frac{J_2^2}{4(J_2 - |J_1|)} & J_2/|J_1| > 2/5 \end{cases}. \tag{3}$$

Importantly, this model contains both first- and second-order phase transitions, which are distinguished by the kind of
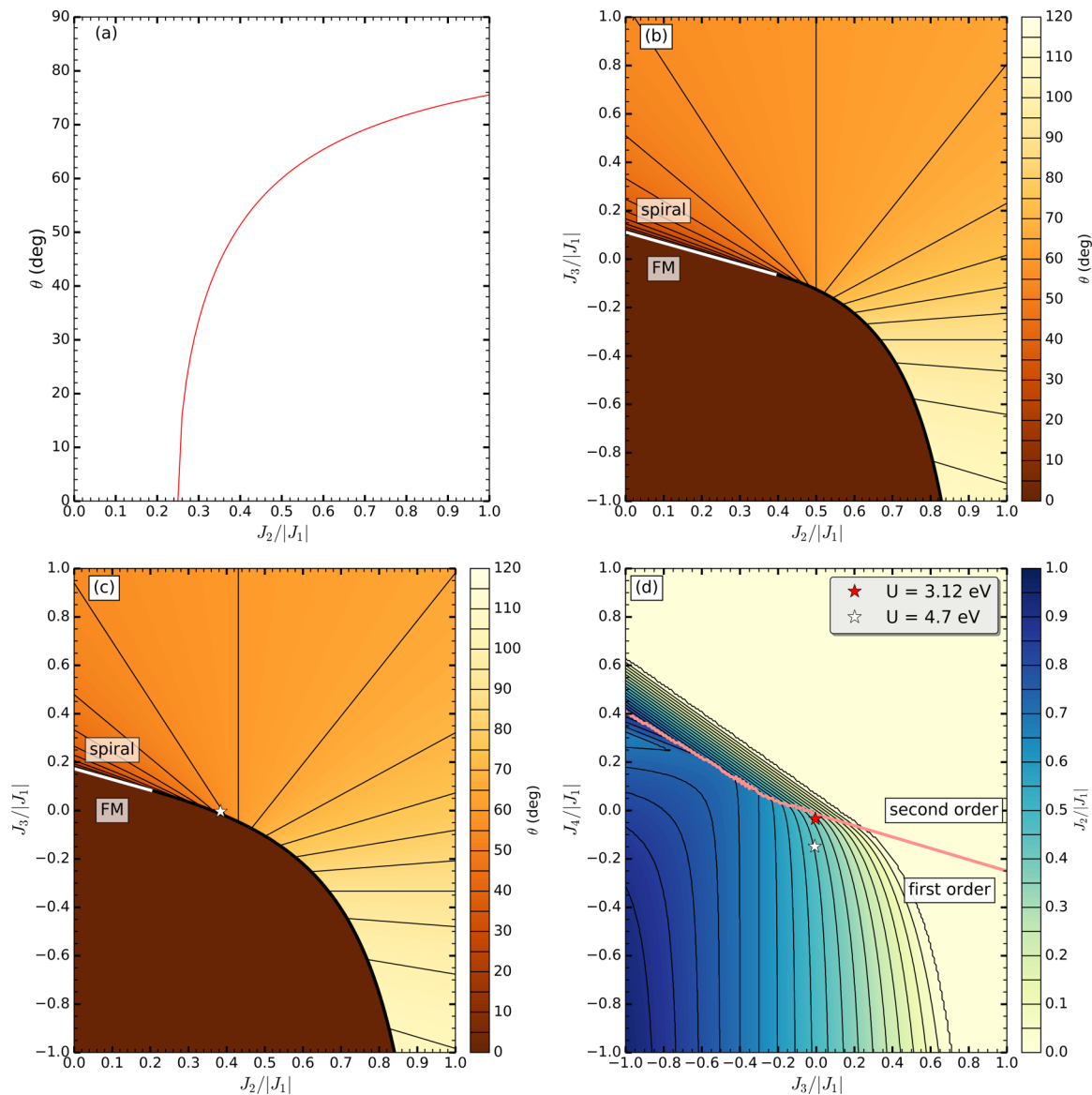
FIG. 1. Phase diagrams for the one-dimensional Heisenberg model of Eq. (1). (a) The phase diagram of the J_1-J_2 model. (b) The phase diagram of the J_1-J_2-J_3 model, where the contour plot corresponds to θ. The thick black line indicates a first-order phase transition and the thick white line indicates a second-order transition. (c) The phase diagram of the J_1-J_2-J_3-J_4 model for $J_4/|J_1| = -0.0346$, plotted in the same manner as panel (b). The white star indicates where ideal stoichiometric MnAu₂ with $U = 3.12$ eV sits in the phase diagram. (d) The critical values of $J_2/|J_1|$ (contour plot), $J_3/|J_1|$, and $J_4/|J_1|$ for the spiral-to-ferromagnetic phase transition. The red line divides parameter space into two regions, where first-order phase transitions occur north of the line, and second-order transitions occur south of it. The red and white stars represent where ideal, stoichiometric MnAu₂ sits for $U = 3.12$ eV and $U = 4.7$ eV, respectively.

degeneracy that occurs on the borders in Eq. (3). A first-order phase transition occurs when there is a degeneracy between the ferromagnetic solution ($\theta = 0$) and a finite angle ($\theta > 0$), while the second order phase transition corresponds to a smooth, continuous connection between ferromagnetic and spin-spiral regions and is found by taking a second-order Maclaurin series expansion of Eq. (2) and equating it with the ferromagnetic solution in the limit $\theta \to 0$. Second-order transitions correspond with the $0 \leqslant J_2/|J_1| \leqslant 2/5$ result and are depicted as the thick white line in Fig. 1(b), while first order transitions correspond to the $J_2/|J_1| > 2/5$ result and are depicted as the thick black line. From this, it is clear that a small ferromagnetic coupling between third-neighbor

planes (relative to $|J_1|$) can change the order of the phase transition.

The analysis is more complicated for four or more neighbor couplings since an analytic solution for θ is not available. Despite this, some properties can still be analytically solved (see Supplemental Material [33]) [24]. The phase boundary for second order transitions is $J_2 = (|J_1| - 9J_3 - 16J_4)/4$. The criterion for a first order phase transition is

$$J_3/|J_1| < -\frac{1 + 64J_4/|J_1|}{15}. \tag{4}$$

Note that the expression for the second order phase boundary and Eq. (4) are valid when $J_3, J_4 > 0$. If one of the parameters

is negative, then the expressions still hold as long as the antiferromagnetic couplings dominate [24], such as $J_3 > 0$, $J_4 < 0$, and $|J_3| \gg |J_4|$. What's clear is that a relatively small fourth neighbor coupling can have a dramatic effect on the location of the first order and second order phase boundaries. To illustrate this, we numerically calculate the phase diagram for the J_1-J_2-J_3-J_4 model with $J_4/|J_1| = -0.0346$, which we plot in Fig. 1(c). Comparing panels (b) and (c), we clearly see that the length of the second order phase boundary (white line) has changed, despite the relative weakness of the fourth neighbor coupling. We also calculate the exchange parameters for ideal, stoichiometric MnAu$_2$ with $U = 3.12$ eV, which are $J_2/|J_1| = 0.3840$, $J_3/|J_1| = -0.0043$, $J_4/|J_1| = -0.0346$, and indicate where MnAu$_2$ sits with the white star. The material sits very close to the first order transition, and a small variation in $J_3/|J_1|$ would drive the system towards ferromagnetism.

In Fig. 1(d) we plot a contour map of the critical values of $J_2/|J_1|$, $J_3/|J_1|$, and $J_4/|J_1|$ for the spiral-to-ferromagnetic transition in the one-dimensional J_1-J_2-J_3-J_4 model. We only consider $J_2 \geqslant 0$ in this figure. The contour plot shows the surface in $(J_2/|J_1|, J_3/|J_1|, J_4/|J_1|)$ space that separates ferromagnetic and spiral order. For example, if you calculate the exchange parameters for MnAu$_2$ and those parameters place the system "inside" the surface ($J_2 < J_2^c$), then the ground state magnetic order is ferromagnetic. If instead the parameters place MnAu$_2$ on or outside the surface ($J_2 \geqslant J_2^c$), then the magnetic order will be a spiral state. Note that the light yellow region corresponding to $J_2^c = 0$ means that the system has spiral order for all $J_2 \geqslant 0$. Finally, if you can tune the parameters, such as by applying pressure or adding holes/electrons, then the system can cross the surface and undergo a phase transition.

As we saw in panels (b) and (c) of Fig. 1, phase transitions can either be first or second order. The parameters $(J_3/|J_1|, J_4/|J_1|)$ control the kind of phase transition that occurs when you cross the surface depicted in Fig. 1(d). The red line separates the first- and second-order transition regions. If you cross the surface while north of the line, then the phase transition is second order; if you cross the surface while south of the line, then the phase transition is first order. Having established this, it is now instructive to indicate where ideal, stoichiometric MnAu$_2$ sits in $(J_3/|J_1|, J_4/|J_1|)$ space for $U = 3.12$ eV (red star) and $U = 4.7$ eV (white star). For both systems, $J_2 > J_2^c$, so they have spiral order. What is striking here is how close MnAu$_2$ sits to the dividing line, especially when $U = 3.12$ eV. This shows that changes in the exchange parameters induced through pressure, doping, or impurities could place the system north of the red line. Since the system sits close to the dividing line, this could explain the discrepancy in experimental pressure studies discussed in Sec. I.

One final point to note is that this analysis assumed that the local moments always have an in-plane orientation. Neutron diffraction experiments confirm that spin spirals in MnAu$_2$ are oriented in-plane [2], and our calculations of the magnetocrystalline anisotropy energy for MnAu$_2$ with $U = 3.12$ eV give $E(001)$–$E(100) = 0.35$ meV [34], indicating the in-plane direction is the preferred axis. Yet, it is less clear what would happen on the first order transition boundary, where zero and finite angle configurations are degenerate. We checked this possibility by considering conical solutions. We added a canted

angle φ and a uniaxial magnetocrystalline anisotropy term to Eq. (2),

$$E(\theta,\varphi) = \text{const} + D\sin^2(\varphi)$$
$$+ \sum_{n=1}^{m} J_n \left[1 - 2\sin^2(\varphi)\sin^2\left(\frac{n\theta}{2}\right) \right]. \quad (5)$$

In this expression, the angles θ and φ remain decoupled and the solutions for θ are unaffected by canting and simple uniaxial magnetocrystalline anisotropy. If we now restrict ourselves to the first-order phase transition boundary, the energy difference between the conical spirals and the ferromagnetic configuration is

$$E(\theta,\varphi) - E(0,\varphi') = D[\sin^2(\varphi) - \sin^2(\varphi')]. \quad (6)$$

Therefore in the absence of magnetocrystalline anisotropy there is a continuous degeneracy of the canting angle. This degeneracy is lifted with the magnetocrystalline anisotropy term, although we should note that the magnetocrystalline anisotropy parameter is small, $D = 0.35$ meV ~ 4 K, and since the pressure experiments [5,21,22] were performed at temperatures of 77 K and at room temperature, it is possible for the ferromagnetic orientation to align along the c axis. It could also be used as a continuous pathway to make θ drop to zero (at finite θ the moments can align parallel to c while on the first-order boundary, and then as you move away from the boundary they can drop back to being in-plane with $\theta = 0$). This means that the phase transition may not be truly first order. However, it should be noted that such a transition entails a rapid change in the canting angle, which would be difficult to distinguish from a first-order transition in experiment. For the rest of the discussion, we will continue to refer to this as a first-order transition with the caveat that it may correspond to a rapid change in the canting angle. Regardless, it remains distinct from the second-order transition, where θ continuously decreases to zero.

IV. DFT RESULTS AND DISCUSSION

Having established in Sec. III that MnAu$_2$ sits close to a dividing line that separates first and second order phase
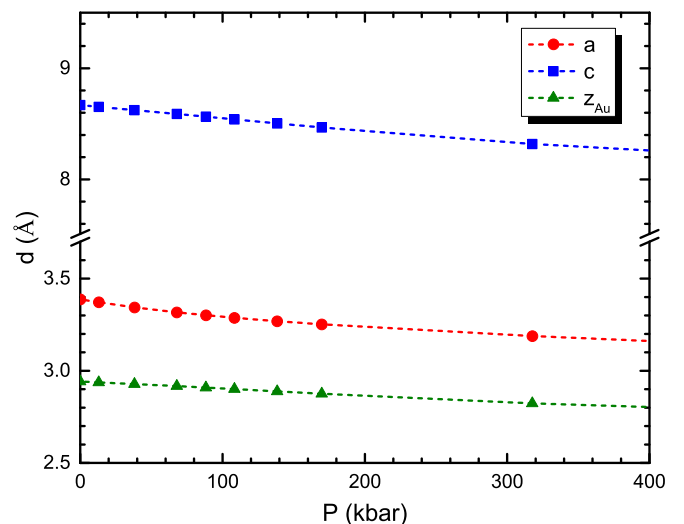

FIG. 2. MnAu$_2$ lattice parameters as a function of pressure.

transitions, we now use DFT to perform a systematic set of spin-spiral calculations to simulate the effects of pressure and doping, and the effect of varying U. This will reveal how applying pressure and doping makes MnAu$_2$ evolve in parameter space. Each set of spin spiral calculations results in a $E(\theta)$ curve, and all curves are similar to what was obtained in our previous paper [19]. Each curve was fitted using the J_1-J_2-J_3-J_4 model, and from these we extract the exchange constants (see Supplemental Material [33]).

It should be noted that these calculations and their subsequent analysis are all done at zero temperature, a choice that we should justify. Measurements of the saturation magnetization at low temperatures ($T \leqslant 10$ K) and at room temperature [35,36], along with measurements of the susceptibility and the critical magnetic field H_c [35], show a very weak dependence on temperature. As discussed in Sec. I, the

temperature dependence of the spiral angle as a function of pressure, obtained using neutron diffraction measurements at 77 K and at room temperature, is also weak [5,6]. The weak temperature dependence of these material parameters suggests that the internal energy determines the important qualitative features of the magnetic phase diagram of MnAu$_2$, and that including thermal fluctuations will result in only minor changes to the area of the spiral and ferromagnetic regions and the length of the first and second order phase boundaries. Therefore, it is reasonable to expect that our conclusions about the spiral-to-ferromagnetic phase transition obtained at zero temperature hold at finite temperatures.

For the pressure calculations, we constrained the volume of our cell and relaxed the structure as described in Sec. II, and then calculated the pressure using the formula $P = -dE/dV$ (see Supplemental Material [33]). Using the LSDA functional

TABLE I. Values of the exchange parameters as a function of pressure, charge dosing, the VCA, and U. Pressure and doping results for $U = 3.12$ eV and $U = 4.7$ eV are reported in the first two sections of the table, where the first five columns are the pressure results and the last six columns are the doping results. The "type" column indicates whether the doping was performed using charge dosing or the VCA. The parameters as a function of U are reported in the last section of the table.

Pressure (kbar)	J_1	J_2 (meV)	J_3	J_4	Doping (elec/Au)	Type	J_1	J_2 (meV)	J_3	J_4
					$U = 3.12$ eV					
0.000	−20.1394	9.8339	−0.9823	−0.7333	−0.050	Dosing	−12.5109	6.7832	−0.5134	−0.6678
12.977	−22.3635	9.9571	−0.7869	−0.7692		VCA	−14.1347	7.1857	−0.5786	−0.6446
38.109	−26.5047	10.1130	−0.4949	−0.7711	−0.025	Dosing	−16.2810	7.1840	−0.2603	−0.6489
67.892	−31.1437	10.2032	−0.2159	−0.6435		VCA	−17.1181	7.3614	−0.3046	−0.6662
88.298	−34.1544	10.3499	−0.1301	−0.6544	0.000	Dosing	−20.2505	7.7762	−0.0861	−0.7000
108.353	−37.0067	10.4056	−0.0440	−0.5633		VCA	−20.2505	7.7762	−0.0861	−0.7000
169.709	−44.9705	10.4817	−0.3415	−0.5701	0.025	Dosing	−24.5855	8.2909	0.3200	−0.7065
						VCA	−23.5647	8.1775	0.3180	−0.6913
					0.050	Dosing	−29.1444	8.4463	0.9843	−0.5759
						VCA	−26.9893	8.2059	0.8370	−0.6678
					$U = 4.7$ eV					
0.000	−5.5435	6.4037	−0.6415	−0.9926	−0.050	Dosing	−0.6574	3.6749	−0.7146	−0.6583
67.892	−13.4226	7.7049	−0.2128	−1.0301		VCA	−1.6202	4.0940	−0.7442	−0.7241
169.709	−24.2692	9.1221	0.0078	−1.0323	−0.025	Dosing	−3.1144	4.3517	−0.3170	−0.9235
200.000	−27.4309	9.6846	0.0290	−1.0575		VCA	−3.6679	4.5317	−0.3207	−0.9799
240.000	−31.4087	10.4061	0.1081	−1.1649	−0.010	Dosing	−4.8464	4.7346	−0.1601	−0.9704
317.691	−39.3228	11.3247	0.2179	−1.1539	−0.005	Dosing	−5.4763	4.9005	−0.0754	−0.9132
					0.000	Dosing	−6.1229	5.0350	−0.0480	−0.9103
						VCA	−6.1229	5.0350	−0.0480	−0.9103
					0.005	Dosing	−6.7465	5.2203	0.0486	−0.8760
					0.010	Dosing	−7.4455	5.4008	0.1156	−0.8414
					0.025	Dosing	−9.6007	5.9304	0.3580	−0.7010
						VCA	−8.8932	5.7378	0.3137	−0.6957
					0.050	Dosing	−13.4470	6.5046	0.6154	−0.4418
						VCA	−11.7329	6.2087	0.6055	−0.4044

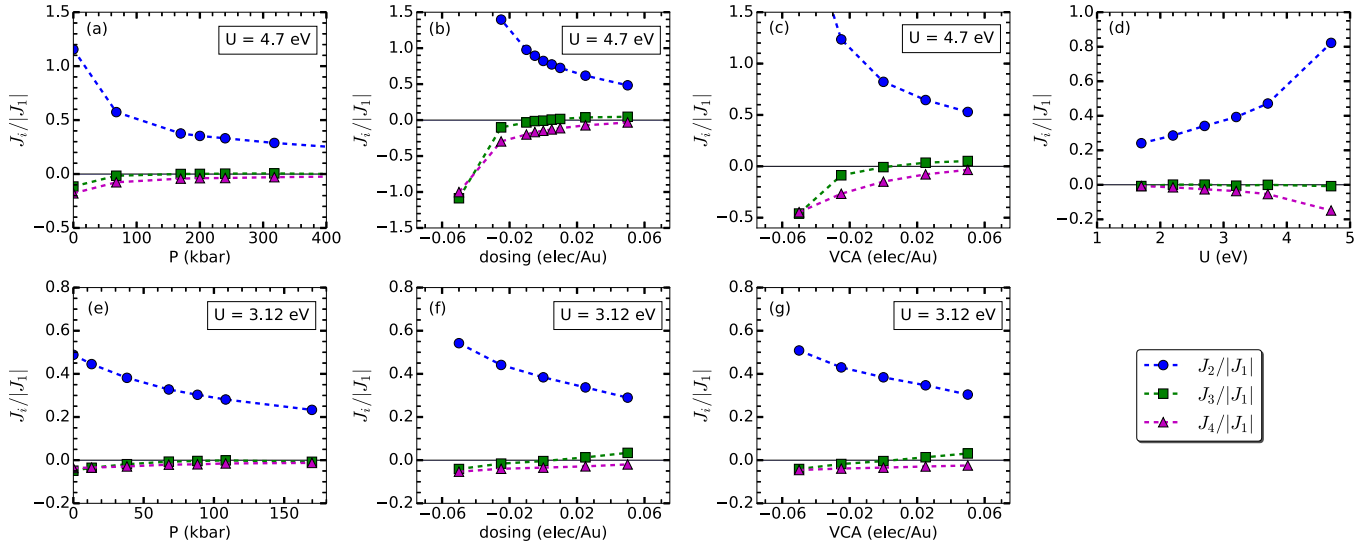| U (eV)	J_1	J_2 (meV)	J_3	J_4
1.7	−37.7314	9.0945	−0.2716	−0.2806
2.2	−31.4231	8.9775	0.0325	−0.4564
2.7	−25.0395	8.5043	0.0267	−0.6542
3.2	−19.4161	7.6273	−0.0997	−0.7022
3.7	−14.3696	6.7687	−0.0028	−0.7722
4.7	−6.1229	5.0350	−0.0480	−0.9103

FIG. 3. The dependence of the exchange parameters $J_2/|J_1|$, $J_3/|J_1|$, and $J_4/|J_1|$, see legend, as a function of pressure, doping, and U. In the charge dosing and VCA panels, positive values on the horizontal axis correspond to electron doping and negative values to hole doping. (a) Pressure dependence with $U = 4.7$ eV. (b) Charge dosing dependence with $U = 4.7$ eV. (c) VCA dependence with $U = 4.7$ eV. (d) Dependence on Hubbard U. (e) Pressure dependence with $U = 3.12$ eV. (f) Charge dosing dependence with $U = 3.12$ eV. (g) VCA dependence with $U = 3.12$ eV.

during relaxation results in overbinding, and so here the equilibrium volume is predicted to be 6% smaller than experiment. To account for this, we shift our pressures such that $P = 0$ corresponds to the experimental volume, and the lattice and internal parameters as a function of pressure are shown in Fig. 2. As the pressure is increased, the parameters decrease in a smooth way, which contrasts with the experimental observation in Ref. [5], which seemed to indicate a sharp drop in the c parameter for $P > 6.5$ kbar [37].

The fitted exchange parameters as functions of pressure, charge dosing, the VCA, and U are reported in Table I. We find that J_1 becomes more ferromagnetic with increasing pressure, electron doping, and decreasing U, and that it is also the most sensitive to these parameters. At 28 kbar of pressure, the absolute value of J_1 grows by 3.0 meV ~ 35 K for $U = 3.12$ eV and 4.5 meV ~ 52 K for $U = 4.7$ eV. In Ref. [21], the critical transition temperature (Néel or Curie, depending on the magnetic state at the given pressure) increases by ~ 40 K
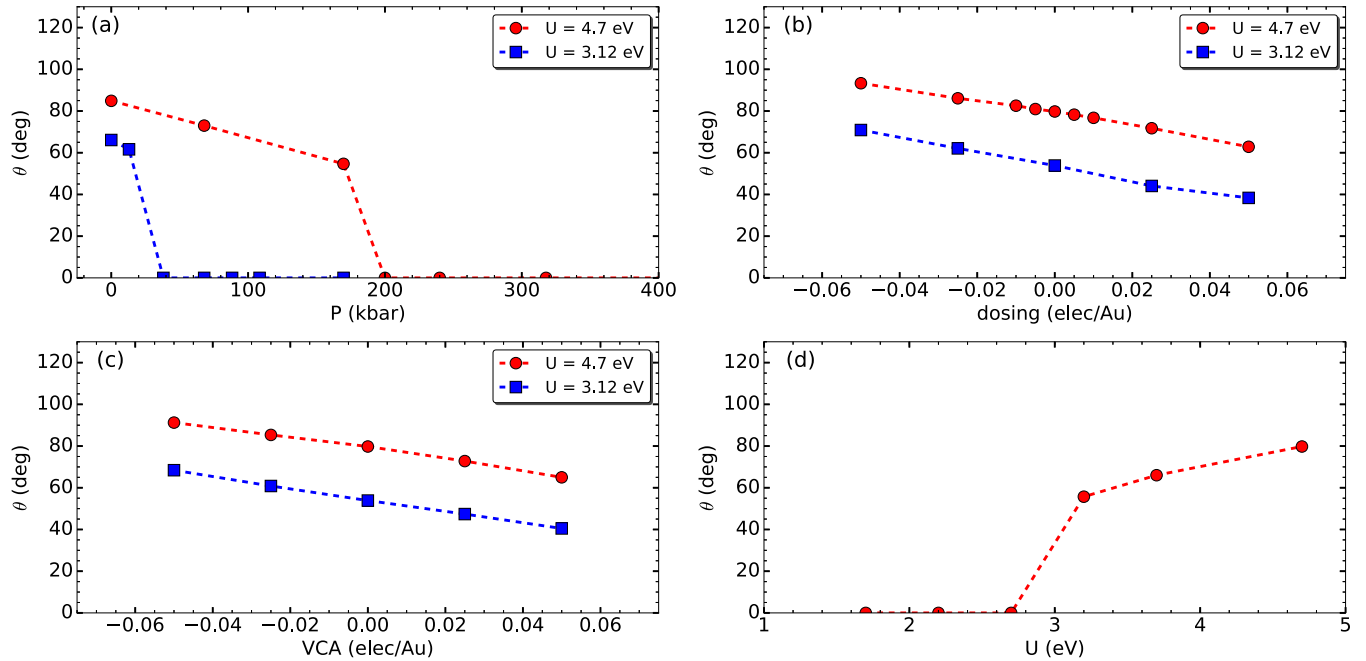

FIG. 4. The spiral angle θ as a function of (a) pressure, (b) charge dosing, (c) the VCA, and (d) U. Panels (a), (b), and (c) include results for $U = 3.12$ eV and 4.7 eV, see legend. The angle θ is obtained by minimizing the J_1-J_2-J_3-J_4 model.

going from zero pressure to 28 kbar, so these changes in J_1 are of the correct order.

To evaluate the spiral-to-ferromagnetic phase transition in the context of the phase diagrams in Fig. 1, we plot the scaled exchange parameters, $j_i \equiv J_i/|J_1|$, in Fig. 3. We find that in all cases j_2 is always antiferromagnetic and is the most sensitive to pressure, doping, and variation in U. j_2 decreases with increasing pressure, electron doping, and decreasing U. The exchange couplings j_3 and j_4 are closer to zero, and do not respond to pressure, doping, and U in the same way as j_2. Applying pressure suppresses j_3, and for $U = 4.7$ eV the cou-

pling becomes slightly antiferromagnetic for $P \gtrsim 170$ kbar. Charge dosing and VCA doping have a stronger effect, where j_3 becomes more ferromagnetic with hole doping (for $U = 4.7$ eV, the coupling becomes enhanced at the large hole doping of -0.05 electrons per Au) and turns antiferromagnetic with electron doping. However, j_3 is insensitive to U, staying close to zero for all considered values. j_4, unlike j_3, remains ferromagnetic in all cases, and often $|j_4| > |j_3|$. Pressure affects j_4 in a similar way as j_3, and for $U = 4.7$ eV so does doping, but for $U = 3.12$ eV, j_4 is less sensitive to doping than j_3. Finally, decreasing U suppresses j_4, going from moderate
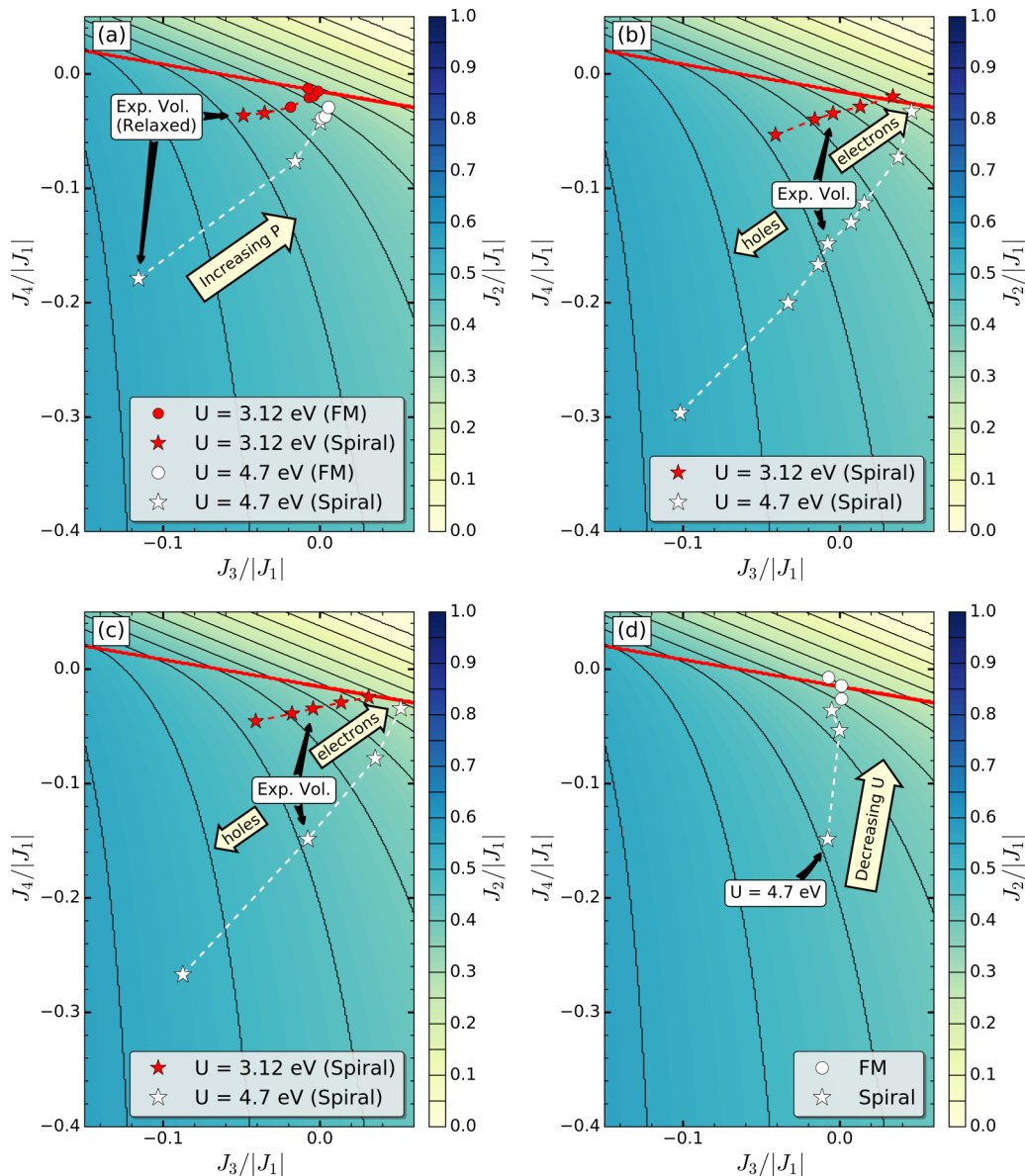

FIG. 5. Parametric plots of the MnAu$_2$ exchange parameters as a function of pressure, doping, and U. The parametric curves are visualized on top of the contour plot from Fig. 1(d). The plot marker shapes indicate the magnetic order of MnAu$_2$, with stars corresponding to spiral order and circles to ferromagnetic order. See legend for the values of U. (a) Parametric curve as a function of pressure. The reference point is the $P = 0$ unit cell, see Fig. 2 for lattice parameters. The arrow indicates the direction of increasing pressure. (b) Parametric curve as a function of charge dosing. The reference point is a unit cell with experimental lattice parameters and no doping. The arrows indicate the direction for increasing electron/hole doping. (c) Parametric curve as a function of the VCA. The reference point is a unit cell with experimental lattice parameters and no doping. The arrows indicate the direction for increasing electron/hole doping. (d) Parametric curve as a function of U. The reference point is a unit cell with experimental parameters and $U = 4.7$ eV. The arrow indicates the direction of decreasing U.

ferromagnetic coupling at $U = 4.7$ eV to being nearly zero at $U = 1.2$ eV. This indicates that measuring the fourth neighbor interplanar coupling in MnAu$_2$ would yield information about the strength of the electronic correlations in this material.

Next we plot θ as a function of pressure, charge dosing, VCA doping, and U in Fig. 4. We obtain θ by minimizing Eq. (2) with the fitted exchange parameters [38]. We find that θ is quite sensitive to pressure, doping, and U. As expected, applying pressure decreases θ in agreement with Ref. [5], and at a critical pressure this induces a phase transition, which is in the range $12.977 \leqslant P \leqslant 38.109$ kbar for $U = 3.12$ eV and $169.709 \leqslant P \leqslant 200$ kbar for $U = 4.7$ eV. This indicates that measurements of the critical pressure provides information about the strength of the electronic correlations. In addition, for both charge dosing and VCA doping the rate of change of θ is independent of U, and θ decreases with electron doping and increases with hole doping. Finally, in Fig. 4(d) we find that θ decreases with decreasing U and eventually collapses to a ferromagnetic state.

The evolution of the magnetic coupling of MnAu$_2$ when subjected to pressure, doping, and variation in U can be further visualized using the contour plot in Fig. 1(d). We take the exchange parameters j_3 and j_4 and plot them as parametric curves on top of the contour plot, which captures how they vary with pressure, doping, and U. For each point, we also compare the fitted j_2 with the critical j_2^c that marks the spiral-to-ferromagnetic phase transition. If $j_2 < j_2^c$, we plot the point as a circle, indicating that the system is ferromagnetic, and if $j_2 \geqslant j_2^c$ we plot the point as a star, which represents spiral order. This procedure yields Fig. 5, and on each panel we give a reference point, which for panel (a) corresponds to the relaxed cell at experimental volume ($P = 0$), for panels (b) and (c) corresponds to the experimental lattice parameters with zero doping, and for panel (d) corresponds to experimental lattice parameters with $U = 4.7$ eV. The arrows with text indicate the direction that the parametric curves evolve, so following the curve from the reference point in panel (a) shows how the parameters change with increasing pressure, in panels (b) and (c) one direction is electron doping and the other is hole doping, and for panel (d) U decreases along the curve. If, while following the curve, the marker symbol changes from a star to a circle, this corresponds to a phase transition. If this change in symbols happens while south of the red line, then the phase transition is first order, and if it happens north of the red line, then it is a second order.

The parametric path for MnAu$_2$ under pressure in Fig. 5(a) shows that the spiral-to-ferromagnetic transition is first order for both values of U. So, for ideal, stoichiometric MnAu$_2$ samples, we expect the pressure-induced phase transition to be of first order, in agreement with Ref. [22]. Decreasing U at ambient pressure also induces a first order phase transition. In contrast, for our considered doping levels MnAu$_2$ does not collapse to the ferromagnetic state. Doping with holes stabilizes the spiral state and drives the system deeper into the first-order parameter region, while doping with electrons moves MnAu$_2$ closer to ferromagnetism and also towards a second-order phase transition. Also, the stronger the correlations, the more dramatic the shifts in parameter space with doping. For both $U = 3.12$ eV and 4.7 eV an electron doping of 0.05 electrons per Au places the system at the dividing

TABLE II. Values of the fitted exchange parameters for the simultaneous pressure and charge dosing calculations. Results are for a charge dosing value of 0.07 electrons per Au and $U = 3.12$ eV.

Pressure	J_1	J_2	J_3	J_4
(kbar)		(meV)		
0.000	−33.5978	10.2441	0.8442	−0.6193
2.000	−33.9957	10.2223	0.8197	−0.6252
6.000	−34.8238	10.1037	0.8679	−0.6570
10.000	−35.6126	10.0322	0.8756	−0.6331
18.000	−37.0886	9.9025	0.9327	−0.6302
20.000	−37.4883	9.8482	0.9131	−0.6498
24.000	−38.1828	9.7781	0.9236	−0.6241

line between first and second order, and it would be expected that the application of pressure for this system would induce a second order transition.

We check the prediction of inducing a second order phase transition by calculating the pressure dependence of MnAu$_2$ with $U = 3.12$ eV and a charge dosing level of 0.07 electrons per Au. The exchange parameters obtained from these calculations are reported in Table II and the scaled exchange parameters, pressure dependence of θ, and a parametric plot of the exchange parameters are plotted in Fig. 6. As shown in Fig. 6(a) the initial charge dosing biases j_2 to be less antiferromagnetic and for j_3 to become more antiferromagnetic. For the range of pressures considered, j_2 decreases with increasing pressure while j_3 and j_4 are unaffected. Figure 6(b) shows the effect this has on the θ vs pressure curve, where the trend of the charge-dosed curve is consistent with a second order phase transition, particularly when compared with the first order transition of the undoped curve included for comparison. The parametric curve in Fig. 6(c) shows that the charge-dosed pressure-dependent path in exchange parameter space is north of the dividing line, confirming the prediction that applying pressure to electron doped MnAu$_2$ can induce a second-order phase transition.

We can use the result that applying pressure to electron-doped MnAu$_2$ induces a second order phase transition to resolve the contradiction in the pressure experiments. In Ref. [21], where the authors found a second order phase transition for MnAu$_2$, they reported that there were trace amounts of MnAu in their sample, such that the system was 34.3% Mn and 65.7% Au. This excess of Mn in their sample can lead to an effective electron doping. Let us assume that the excess Mn atoms are also in the 2+ ionic charge state, and that the extra electrons they donate are spread homogeneously over the system. This would mean that each unit cell of MnAu$_2$ would have 2 electrons per Mn · (34.3/33.3) = 2.06 electrons per Mn, or an excess of 0.03 electrons per Au. Assuming that $U = 3.12$ eV [39] and comparing with the electron dosing curve in Fig. 5(b), an extra 0.03 electrons per Au would shift the sample near the second order transition region of the parameter space, which as we've seen can lead to a second order phase transition upon application of pressure. While the MnAu domains are not likely to uniformly dope the material, we see how the variations in sample quality can influence the kind of phase transition. This stresses both the
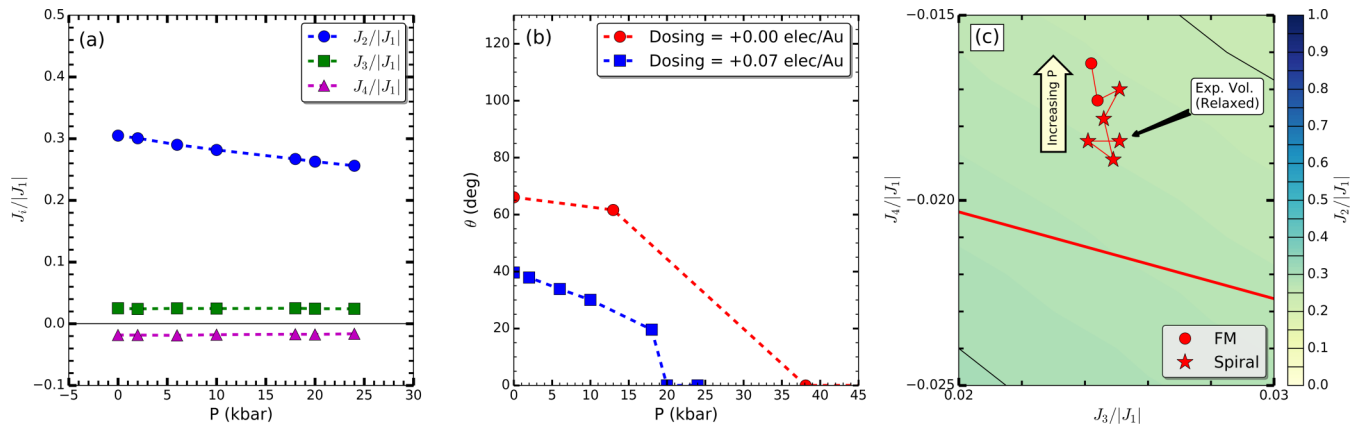
FIG. 6. Plots showing the results of calculations with simultaneous charge dosing and applied pressure. The calculations were performed using $U = 3.12$ eV and a charge dosing of 0.07 electrons per Au. (a) The exchange parameters $J_2/|J_1|$, $J_3/|J_1|$, and $J_4/|J_1|$, see legend, as a function of pressure. (b) The spiral angle θ as a function of pressure with and without charge dosing, see the legend. (c) Parametric plot of the exchange parameters as a function of pressure visualized on top of the contour plot from Fig. 1(d). The plot markers indicate the type of magnetic order, see the legend. The reference point is the relaxed $P = 0$ unit cell. The arrow indicates the direction of increasing pressure.

importance of controlling for impurities in MnAu$_2$ and that the magnetic properties are also amenable to tuning.

V. CONCLUSIONS

We studied how the magnetic exchange in MnAu$_2$ changes upon application of pressure and doping using a series of DFT calculations, as well as varying the electronic correlations with a Hubbard-like U. We found that the proper model for these interactions is the one-dimensional Heisenberg model with coupling between the first *four* Mn planes (the J_1-J_2-J_3-J_4 model), which contrasts with previous studies that only considered interactions between the first two planes. Within this model, transitions between the ferromagnetic and spiral phases can be either first or second order, and J_3 and J_4 control the order of the phase transition. Our analysis finds that ideal, stoichiometric MnAu$_2$ sits near a dividing line in (J_3, J_4) space that separates first- and second-order phase transitions. Applying pressure collapses the spiral state as expected, and for ideal, stoichiometric MnAu$_2$ the transition is first order. Hole doping the material further stabilizes the spiral and the tendency towards a first-order transition. In contrast, electron doping the material makes the spiral less stable and moves

the system in (J_3, J_4) space closer to a second-order transition. We confirm with additional DFT calculations that applying pressure to electron-doped MnAu$_2$ will induce a second-order phase transition. Therefore, impurities that provide an effective electron doping, such as excess Mn, can cause the spiral-to-ferromagnetic phase transition to become second order under pressure. These results indicate that MnAu$_2$ is tunable, where the kind of phase transition can be set and the spiral angle controlled through both pressure and doping, which can include gate voltages. The ability to control the spiral angle holds promise for integration of MnAu$_2$ in spintronics devices, such as in a spin valve. Attaching a thin film of MnAu$_2$ to the free magnetic layer of a spin valve and then applying a gate voltage could allow for a current-free manipulation of the relative orientation between the free and pinned magnetic layers, which would reduce Joule heating and could help in developing smaller-scale electronics devices.

ACKNOWLEDGMENTS

[1] A. J. Meyer and P. Taglang, J. Phys. Radium **17**, 457 (1956).

[2] A. Herpin, P. Meriel, and J. Villain, Comptes Rendus **249**, 1334 (1959).

[3] A. Herpin and P. Meriel, J. Phys. Radium **22**, 337 (1961).

[4] H. Samata, N. Sekiguchi, A. Sawabe, Y. Nagata, T. Uchida, and M. D. Lan, J. Phys. Chem. Solids **59**, 377 (1998).

[5] F. A. Smith, C. C. Bradley, and G. E. Bacon, J. Phys. Chem. Solids **27**, 925 (1966).

[6] A. Handstein, U. K. Rößler, B. Idzikowski, N. Kozlova, K. Nenkov, K. H. Müller, A. Kreyssig, M. Loewenhaupt, A. Heinemann, A. Hoell, and N. Stüßer, J. Magn. Magn. Mater. **290-291** (Part 2), 1093 (2005).

[7] W. E. Evenson and S. H. Liu, Phys. Rev. Lett. **21**, 432 (1968).

[8] M. A. Ruderman and C. Kittel, Phys. Rev. **96**, 99 (1954).

[9] T. Kasuya, Prog. Theor. Phys. **16**, 45 (1956).

[10] K. Yosida, Phys. Rev. **106**, 893 (1957).

[11] I. Dzyaloshinsky, J. Phys. Chem. Solids **4**, 241 (1958).

[12] T. Moriya, Phys. Rev. **120**, 91 (1960).

[13] P. Bak and M. H. Jensen, J. Phys. C **13**, L881 (1980).

[14] O. Nakanishi, A. Yanase, A. Hasegawa, and M. Kataoka, Solid State Commun. **35**, 995 (1980).

[15] M. Kataoka and O. Nakanishi, J. Phys. Soc. Jpn. **50**, 3888 (1981).

[16] U. Enz, J. Appl. Phys. **32**, S22 (1961).

[17] T. Nagamiya, J. Appl. Phys. **33**, 1029 (1962).

[18] L. Udvardi, S. Khmelevskyi, L. Szunyogh, P. Mohn, and P. Weinberger, Phys. Rev. B **73**, 104446 (2006).

[19] J. K. Glasbrenner, K. M. Bussmann, and I. I. Mazin, Phys. Rev. B **90**, 144421 (2014).

[20] N. P. Grazhdankina and K. P. Rodionov, Sov. Phys. JETP **16**, 1429 (1963).

[21] R. C. Wayne and F. A. Smith, J. Phys. Chem. Solids **30**, 183 (1969).

[22] R. Adiatullin and I. G. Fakidov, Sov. Phys. Solid State **12**, 2547 (1971).

[23] A. Pimpinelli, E. Rastelli, and A. Tassi, J. Phys.: Condens. Matter **1**, 7941 (1989).

[24] R. Zinke, J. Richter, and S.-L. Drechsler, J. Phys.: Condens. Matter **22**, 446002 (2010).

[25] ELK FP-LAPW Code, http://elk.sourceforge.net/.

[26] G. Kresse and J. Hafner, Phys. Rev. B **47**, 558(R) (1993).

[27] G. Kresse and J. Furthmüller, Phys. Rev. B **54**, 11169 (1996).

[28] J. P. Perdew and Y. Wang, Phys. Rev. B **45**, 13244 (1992).

[29] A. I. Liechtenstein, V. I. Anisimov, and J. Zaanen, Phys. Rev. B **52**, R5467(R) (1995).

[30] K. Adachi, K. Sato, H. Watarai, and T. Ido, J. Phys. Soc. Jpn. **32**, 572 (1972).

[31] L. W. Hart and J. L. Stanford, J. Appl. Phys. **41**, 2523 (1970).

[32] The experimental pressure studies of $MnAu_2$ do not find changes in the crystal structure prior to the spiral-to-ferromagnetic phase transition. For this reason, we only investigate tetragonal unit cells and do not consider whether other structures become competitive at higher pressures, since they will not impact the phase transition.

[33] See Supplemental Material at http://link.aps.org/supplemental/10.1103/PhysRevB.93.184402 for our raw data and a Jupyter (formerly IPython) notebook that describes the published research in full detail. The goal of including this material is so that readers can verify and reproduce all the presented results. The notebook contains all the Python code used to analyze our DFT calculations and produce the figures and tables contained in the paper. The notebook also contains some additional calculations and diagrams not presented in the main text that, while not essential for our arguments, may be of interest to the reader. Specifically, the notebook contains: (1) an annotated analysis of the results of structural optimizations performed in VASP, (2) a full and annotated derivation of the analytic results of the one-dimensional Heisenberg model, (3) details of how we fit our results to the one-dimensional J_1-J_2-J_3-J_4 Heisenberg model, and (4) how we created the contour plots, phase diagrams, and visualized the exchange parameters and spiral angle θ as a function of pressure, doping, and U.

[34] Convergence of the magnetocrystalline anisotropy energy in the $MnAu_2$ unit cell was achieved with the following parameters in ELK: k-mesh = 28×28×28, nempty = 12, rgkmax = 8.0, gmaxvr = 16, lmaxapw = 14, lmaxvr = 14, and the smearing function width was set to 0.0001 Ha.

[35] Y. Nagata, T. Hagii, H. Samata, T. Uchida, S. Abe, C. Fan Sung, and M. Der Lan, J. Alloys Compd. **284**, 47 (1999).

[36] A. Handstein, K. Nenkov, U. K. Rössler, and K.-H. Müller, J. Appl. Phys. **87**, 5789 (2000).

[37] There is a large error in measuring c as a function of pressure in Ref. [5], so it is likely that the reported drop is not a real effect.

[38] We note that an alternative approach is to interpolate $E(\theta)$ and find the minimum, and away from phase transitions these two methods are in good agreement (see Supplemental Material [33]). However, near a phase transition the energy wells become shallow and the interpolations are no longer reliable, so for consistency we report results obtained by minimizing Eq. (2).

[39] This choice of U yields a $\theta < 60°$ and a critical transition pressure $P \sim 20$–40 kbar, in reasonable agreement with experiment.